The Astrophysical Journal, 696:L150–L155, 2009 May 10 doi:10.1088/0004-637X/696/2/L150

SIMULTANEOUS OBSERVATIONS OF PKS 2155−304 WITH HESS, *FERMI*, *RXTE*, AND ATOM: SPECTRAL ENERGY DISTRIBUTIONS AND VARIABILITY IN A LOW STATE

F. Aharonian[1,2], A. G. Akhperjanian[3], G. Anton[4], U. Barres de Almeida[5,76], A. R. Bazer-Bachi[6], Y. Becherini[7,8], B. Behera[9], K. Bernlöhr[1,10], C. Boisson[11], A. Bochow[1], V. Borrel[6], E. Brion[12], J. Brucker[4], P. Brun[12], R. Bühler[1], T. Bulik[13], I. Büsching[14], T. Boutelier[15], P. M. Chadwick[5], A. Charbonnier[16], R. C. G. Chaves[1], A. Cheesebrough[5], L.-M. Chounet[17], A. C. Clapson[1], G. Coignet[18], M. Dalton[10], M. K. Daniel[5], I. D. Davids[14,19], B. Degrange[17], C. Deil[1], H. J. Dickinson[5], A. Djannati-Ataï[7,8], W. Domainko[1], L. O'C. Drury[2], F. Dubois[18], G. Dubus[15], J. Dyks[13], M. Dyrda[20], K. Egberts[1], D. Emmanoulopoulos[9], P. Espigat[7,8], C. Farnier[21], F. Feinstein[21], A. Fiasson[21], A. Förster[1], G. Fontaine[17], M. Füssling[10], S. Gabici[2], Y. A. Gallant[21], L. Gérard[7,8,77], B. Giebels[17,77], J. F. Glicenstein[12], B. Glück[4], P. Goret[12], D. Göhring[4], D. Hauser[9], M. Hauser[9], S. Heinz[4], G. Heinzelmann[22], G. Henri[15], G. Hermann[1], J. A. Hinton[23], A. Hoffmann[24], W. Hofmann[1], M. Holleran[14], S. Hoppe[1], D. Horns[22], A. Jacholkowska[16], O. C. de Jager[14], C. Jahn[4], I. Jung[4], K. Katarzyński[25], U. Katz[4], S. Kaufmann[9], E. Kendziorra[24], M. Kerschhaggl[10], D. Khangulyan[1], B. Khélifi[17], D. Keogh[5], W. Kluźniak[13], Nu. Komin[12], K. Kosack[1], G. Lamanna[18], J.-P. Lenain[11], T. Lohse[10], V. Marandon[7,8], J. M. Martin[11], O. Martineau-Huynh[16], A. Marcowith[21], D. Maurin[16], T. J. L. McComb[5], M. C. Medina[11], R. Moderski[13], E. Moulin[12], M. Naumann-Godo[17], M. de Naurois[16], D. Nedbal[26], D. Nekrassov[1], J. Niemiec[20], S. J. Nolan[5], S. Ohm[1], J-F. Olive[6], E. de Oña Wilhelmi[7,8,78], K. J. Orford[5], M. Ostrowski[27], M. Panter[1], M. Paz Arribas[10], G. Pedaletti[9], G. Pelletier[15], P.-O. Petrucci[15], S. Pita[7,8], G. Pühlhofer[9], M. Punch[7,8], A. Quirrenbach[9], B. C. Raubenheimer[14], M. Raue[1,77], S. M. Rayner[5], M. Renaud[1,7,8], F. Rieger[1,77], J. Ripken[22], L. Rob[26], S. Rosier-Lees[18], G. Rowell[28], B. Rudak[13], C. B. Rulten[5], J. Ruppel[29], V. Sahakian[3], A. Santangelo[24], R. Schlickeiser[29], F. M. Schöck[4], R. Schröder[29], U. Schwanke[10], S. Schwarzburg[24], S. Schwemmer[9], A. Shalchi[29], M. Sikora[13], J. L. Skilton[23], H. Sol[11], D. Spangler[5], Ł Stawarz[27], R. Steenkamp[19], C. Stegmann[4], G. Superina[17], A. Szostek[27,15], P. H. Tam[9], J.-P. Tavernet[16], R. Terrier[7,8], O. Tibolla[1,9], C. van Eldik[1], G. Vasileiadis[21], C. Venter[14], L. Venter[11], J. P. Vialle[18], P. Vincent[16], M. Vivier[12], H. J. Völk[1], F. Volpe[1,17,77], S. J. Wagner[9], M. Ward[5], A. A. Zdziarski[13], A. Zech[11] (The HESS Collaboration), A. A. Abdo[30], M. Ackermann[31], M. Ajello[31], W. B. Atwood[32], M. Axelsson[33,34], L. Baldini[35], J. Ballet[36], G. Barbiellini[37,38], M. G. Baring[39], D. Bastieri[40,41], M. Battelino[33,42], B. M. Baughman[43], K. Bechtol[31], R. Bellazzini[35], B. Berenji[31], E. D. Bloom[31], E. Bonamente[44,45], A. W. Borgland[31], J. Bregeon[35], A. Brez[35], M. Brigida[46,47], P. Bruel[17], G. A. Caliandro[46,47], R. A. Cameron[31], P. A. Caraveo[48], J. M. Casandjian[36], E. Cavazzuti[49], C. Cecchi[44,45], E. Charles[31], A. Chekhtman[50,30], A. W. Chen[48], C. C. Cheung[51], J. Chiang[31,76], S. Ciprini[44,45], R. Claus[31], J. Cohen-Tanugi[21], S. Colafrancesco[49], J. Conrad[33,42,52], L. Costamante[31], S. Cutini[49], C. D. Dermer[30], A. de Angelis[53], F. de Palma[46,47], S. W. Digel[31], E. do Couto e Silva[31], P. S. Drell[31], R. Dubois[31], G. Dubus[15], D. Dumora[54,55], C. Farnier[21], C. Favuzzi[46,47], S. J. Fegan[17], E. C. Ferrara[51], P. Fleury[17], W. B. Focke[31], M. Frailis[53], Y. Fukazawa[56], S. Funk[31], P. Fusco[46,47], F. Gargano[47], D. Gasparrini[49], N. Gehrels[51,57], S. Germani[44,45], B. Giebels[17,77], N. Giglietto[46,47], F. Giordano[46,47], M.-H. Grondin[55,58], J. E. Grove[30], L. Guillemot[55,58], S. Guiriec[21], Y. Hanabata[56], A. K. Harding[51], M. Hayashida[31], E. Hays[51], D. Horan[17], G. Jóhannesson[31], A. S. Johnson[31], R. P. Johnson[32], W. N. Johnson[30], M. Kadler[59,60,61,62], T. Kamae[31], H. Katagiri[56], J. Kataoka[63], M. Kerr[64], J. Knödlseder[6], F. Kuehn[43], M. Kuss[35], J. Lande[31], L. Latronico[35], S.-H. Lee[31], M. Lemoine-Goumard[55,58], F. Longo[37,38], F. Loparco[46,47], B. Lott[55,58], M. N. Lovellette[30], G. M. Madejski[31], A. Makeev[30,50], M. N. Mazziotta[47], J. E. McEnery[51], C. Meurer[33,52], P. F. Michelson[31], W. Mitthumsiri[31], T. Mizuno[56], A. A. Moiseev[60], C. Monte[46,47], M. E. Monzani[31], A. Morselli[65], I. V. Moskalenko[31], S. Murgia[31], P. L. Nolan[31], E. Nuss[21], T. Ohsugi[56], N. Omodei[35], E. Orlando[66], J. F. Ormes[67], D. Paneque[31], J. H. Panetta[31], D. Parent[55,58], V. Pelassa[21], M. Pepe[44,45], M. Pesce-Rollins[35], F. Piron[21], T. A. Porter[32], S. Rainò[46,47], M. Razzano[35], A. Reimer[31], O. Reimer[31], T. Reposeur[55,58], S. Ritz[51,57], A. Y. Rodriguez[68], F. Ryde[33,42], H. F.-W. Sadrozinski[32], D. Sanchez[17,77], A. Sander[43], J. D. Scargle[69], T. L. Schalk[32], A. Sellerholm[33,52], C. Sgrò[35], M. Shaw[31], D. A. Smith[55,58], G. Spandre[35], P. Spinelli[46,47], J.-L. Starck[36], M. S. Strickman[30], H. Tajima[31], H. Takahashi[56], T. Takahashi[70], T. Tanaka[31], J. G. Thayer[31], D. J. Thompson[51], L. Tibaldo[40,41], D. F. Torres[68,71], G. Tosti[44,45], A. Tramacere[31,72], Y. Uchiyama[31], T. L. Usher[31], N. Vilchez[6], M. Villata[73], V. Vitale[65,74], A. P. Waite[31], K. S. Wood[30], T. Ylinen[33,42,75], and M. Ziegler[32] (The *Fermi*–LAT Collaboration)

[1] Max-Planck-Institut für Kernphysik, P.O. Box 103980, D-69029 Heidelberg, Germany
[2] Dublin Institute for Advanced Studies, 5 Merrion Square, Dublin 2, Ireland
[3] Yerevan Physics Institute, 2 Alikhanian Brothers Street, 375036 Yerevan, Armenia
[4] Universität Erlangen-Nürnberg, Physikalisches Institut, Erwin-Rommel-Str. 1, D-91058 Erlangen, Germany
[5] University of Durham, Department of Physics, South Road, Durham DH1 3LE, UK
[6] Centre d'Étude Spatiale des Rayonnements, CNRS/UPS, BP 44346, F-31028 Toulouse Cedex 4, France
[7] Astroparticule et Cosmologie (APC), CNRS, Universite Paris 7 Denis Diderot, 10, rue Alice Domon et Leonie Duquet, F-75205 Paris Cedex 13, France; lucie.gerard@apc.univ-paris7.fr
[8] UMR 7164 (CNRS, Université Paris VII, CEA, Observatoire de Paris), Paris, France
[9] Landessternwarte, Universität Heidelberg, Königstuhl, D-69117 Heidelberg, Germany
[10] Institut für Physik, Humboldt-Universität zu Berlin, Newtonstr. 15, D-12489 Berlin, Germany
[11] LUTH, Observatoire de Paris, CNRS, Université Paris Diderot, 5 Place Jules Janssen, 92190 Meudon, France
[12] IRFU/DSM/CEA, CE Saclay, F-91191 Gif-sur-Yvette, Cedex, France

[13] Nicolaus Copernicus Astronomical Center, ul. Bartycka 18, 00-716 Warsaw, Poland
[14] Unit for Space Physics, Northwest University, Potchefstroom 2520, South Africa
[15] Laboratoire d'Astrophysique de Grenoble, INSU/CNRS, Université Joseph Fourier, BP 53, F-38041 Grenoble Cedex 9, France
[16] LPNHE, Université Pierre et Marie Curie Paris 6, Université Denis Diderot Paris 7, CNRS/IN2P3, 4 Place Jussieu, F-75252, Paris Cedex 5, France
[17] Laboratoire Leprince-Ringuet, École polytechnique, CNRS/IN2P3, Palaiseau, France; berrie@in2p3.fr, sanchez@poly.in2p3.fr
[18] Laboratoire d'Annecy-le-Vieux de Physique des Particules, CNRS/IN2P3, 9 Chemin de Bellevue-BP 110 F-74941 Annecy-le-Vieux Cedex, France
[19] University of Namibia, Private Bag 13301, Windhoek, Namibia
[20] Instytut Fizyki Jądrowej PAN, ul. Radzikowskiego 152, 31-342 Kraków, Poland
[21] Laboratoire de Physique Théorique et Astroparticules, Université Montpellier 2, CNRS/IN2P3, Montpellier, France
[22] Universität Hamburg, Institut für Experimentalphysik, Luruper Chaussee 149, D-22761 Hamburg, Germany
[23] School of Physics & Astronomy, University of Leeds, Leeds LS2 9JT, UK
[24] Institut für Astronomie und Astrophysik, Universität Tübingen, Sand 1, D-72076 Tübingen, Germany
[25] Toruń Centre for Astronomy, Nicolaus Copernicus University, ul. Gagarina 11, 87-100 Toruń, Poland
[26] Institute of Particle and Nuclear Physics, Charles University, V Holesovickach 2, 180 00 Prague 8, Czech Republic
[27] Obserwatorium Astronomiczne, Uniwersytet Jagielloński, ul. Orla 171, 30-244 Kraków, Poland
[28] School of Chemistry & Physics, University of Adelaide, Adelaide 5005, Australia
[29] Institut für Theoretische Physik, Lehrstuhl IV, Weltraum und Astrophysik, Ruhr-Universität Bochum, D-44780 Bochum, Germany
[30] Space Science Division, Naval Research Laboratory, Washington, DC 20375, USA
[31] W. W. Hansen Experimental Physics Laboratory, Kavli Institute for Particle Astrophysics and Cosmology, Department of Physics and Stanford Linear Accelerator Center, Stanford University, Stanford, CA 94305, USA; jchiang@slac.stanford.edu
[32] Santa Cruz Institute for Particle Physics, Department of Physics and Department of Astronomy and Astrophysics, University of California at Santa Cruz, Santa Cruz, CA 95064, USA
[33] The Oskar Klein Centre for Cosmo Particle Physics, AlbaNova, SE-106 91 Stockholm, Sweden
[34] Stockholm Observatory, Albanova, SE-106 91 Stockholm, Sweden
[35] Istituto Nazionale di Fisica Nucleare, Sezione di Pisa, I-56127 Pisa, Italy
[36] Laboratoire AIM, CEA-IRFU/CNRS/Université Paris Diderot, Service d'Astrophysique, CEA Saclay, 91191 Gif sur Yvette, France
[37] Istituto Nazionale di Fisica Nucleare, Sezione di Trieste, I-34127 Trieste, Italy
[38] Dipartimento di Fisica, Università di Trieste, I-34127 Trieste, Italy
[39] Rice University, Department of Physics and Astronomy, MS-108, P.O. Box 1892, Houston, TX 77251, USA
[40] Istituto Nazionale di Fisica Nucleare, Sezione di Padova, I-35131 Padova, Italy
[41] Dipartimento di Fisica "G. Galilei," Università di Padova, I-35131 Padova, Italy
[42] Department of Physics, Royal Institute of Technology (KTH), AlbaNova, SE-106 91 Stockholm, Sweden
[43] Department of Physics, Center for Cosmology and Astro-Particle Physics, The Ohio State University, Columbus, OH 43210, USA
[44] Istituto Nazionale di Fisica Nucleare, Sezione di Perugia, I-06123 Perugia, Italy
[45] Dipartimento di Fisica, Università degli Studi di Perugia, I-06123 Perugia, Italy
[46] Dipartimento di Fisica "M. Merlin" dell'Università e del Politecnico di Bari, I-70126 Bari, Italy
[47] Istituto Nazionale di Fisica Nucleare, Sezione di Bari, 70126 Bari, Italy
[48] INAF-Istituto di Astrofisica Spaziale e Fisica Cosmica, I-20133 Milano, Italy
[49] Agenzia Spaziale Italiana (ASI) Science Data Center, I-00044 Frascati (Roma), Italy
[50] George Mason University, Fairfax, VA 22030, USA
[51] NASA Goddard Space Flight Center, Greenbelt, MD 20771, USA
[52] Department of Physics, Stockholm University, AlbaNova, SE-106 91 Stockholm, Sweden
[53] Dipartimento di Fisica, Università di Udine and Istituto Nazionale di Fisica Nucleare, Sezione di Trieste, Gruppo Collegato di Udine, I-33100 Udine, Italy
[54] Université de Bordeaux, Centre d'Études Nucléaires Bordeaux Gradignan, UMR 5797, Gradignan 33175, France
[55] Department of Physical Science and Hiroshima Astrophysical Science Center, Hiroshima University, Higashi-Hiroshima 739-8526, Japan
[56] University of Maryland, College Park, MD 20742, USA
[57] CNRS/IN2P3, Centre d'Études Nucléaires Bordeaux Gradignan, UMR 5797, Gradignan 33175, France
[58] Dr. Remeis-Sternwarte Bamberg, Sternwartstrasse 7, D-96049 Bamberg, Germany
[59] Center for Research and Exploration in Space Science and Technology (CRESST), NASA Goddard Space Flight Center, Greenbelt, MD 20771, USA
[60] Erlangen Centre for Astroparticle Physics, D-91058 Erlangen, Germany
[61] Universities Space Research Association (USRA), Columbia, MD 21044, USA
[62] Department of Physics, Tokyo Institute of Technology, Meguro City, Tokyo 152-8551, Japan
[63] Department of Physics, University of Washington, Seattle, WA 98195-1560, USA
[64] Istituto Nazionale di Fisica Nucleare, Sezione di Roma "Tor Vergata," I-00133 Roma, Italy
[65] Max-Planck Institut für Extraterrestrische Physik, 85748 Garching, Germany
[66] Department of Physics and Astronomy, University of Denver, Denver, CO 80208, USA
[67] Institut de Ciencies de l'Espai (IEEC-CSIC), Campus UAB, 08193 Barcelona, Spain
[68] Space Sciences Division, NASA Ames Research Center, Moffett Field, CA 94035-1000, USA
[69] Institute of Space and Astronautical Science, JAXA, 3-1-1 Yoshinodai, Sagamihara, Kanagawa 229-8510, Japan
[70] Institució Catalana de Recerca i Estudis Avançats (ICREA), Barcelona, Spain
[71] Consorzio Interuniversitario per la Fisica Spaziale (CIFS), I-10133 Torino, Italy
[72] INAF, Osservatorio Astronomico di Torino, I-10025 Pino Torinese (TO), Italy
[73] Dipartimento di Fisica, Università di Roma "Tor Vergata," I-00133 Roma, Italy
[74] School of Pure and Applied Natural Sciences, University of Kalmar, SE-391 82 Kalmar, Sweden
Received 2009 January 26; accepted 2009 March 16; published 2009 April 24

ABSTRACT

We report on the first simultaneous observations that cover the optical, X-ray, and high-energy gamma-ray bands of the BL Lac object PKS 2155−304. The gamma-ray bands were observed for 11 days, between 2008 August 25 and 2008 September 6 (MJD 54704−54715), jointly with the *Fermi Gamma-ray Space Telescope* and the HESS atmospheric Cherenkov array, providing the first simultaneous MeV–TeV spectral energy distribution (SED) with the new generation of γ-ray telescopes. The ATOM telescope and the *RXTE* and *Swift* observatories provided optical and

X-ray coverage of the low-energy component over the same time period. The object was close to the lowest archival X-ray and very high energy (VHE; >100 GeV) state, whereas the optical flux was much higher. The light curves show relatively little (∼30%) variability overall when compared to past flaring episodes, but we find a clear optical/VHE correlation and evidence for a correlation of the X-rays with the high-energy spectral index. Contrary to previous observations in the flaring state, we do not find any correlation between the X-ray and VHE components. Although synchrotron self-Compton models are often invoked to explain the SEDs of BL Lac objects, the most common versions of these models are at odds with the correlated variability we find in the various bands for PKS 2155−304.

Key words: BL Lacertae objects: individual (PKS 2155−304) – galaxies: active – gamma rays: observations

1. INTRODUCTION

The underlying particle distributions of blazars are usually studied by matching broadband observations with predictions from radiative models. Since these sources are highly variable, simultaneous observations are essential. The most energetic BL Lac spectra extend up to TeV energies, and positive detections have usually indicated flaring states. However, with their improved sensitivity, the new generation of Atmospheric Cherenkov Telescopes (ACTs), which has more than quadrupled[79] the number of known extragalactic very high energy (VHE) sources, finds a few of these sources in marginally variable states with consistent detections after short exposures. One of these objects, the blazar PKS 2155−304 at $z = 0.116$, is an ideal target for such studies. Crucial information is expected from the *Fermi* Gamma-ray Space Telescope, since its improved sensitivity over EGRET would constrain dramatically the existing models that predict a wide variety of fluxes in the 100 MeV–10 TeV energy range. Since the HESS experiment detects this source in a low state within ∼1 hr, significant daily detections were guaranteed and the source was targeted for an 11-day multiwavelength campaign.

2. OBSERVATIONS AND ANALYSIS RESULTS

The HESS observations of PKS 2155−304 took place during MJD 54701−54715, for a total of 42.2 hr. After applying the standard HESS data-quality selection criteria, an exposure of 32.9 hr live time remains (MJD 54704−54715), at a mean zenith angle of 18°.3. The data set has been calibrated using the standard HESS calibration method (Aharonian et al. 2004). The analysis tools and the event-selection criteria used for the VHE analysis are presented in F. Aharonian et al. (2009, in preparation). The events have been selected using "loose cuts," preferred for their lower energy threshold of 200 GeV and higher γ-ray acceptance. A 0°.2 radius circular region centered on PKS 2155−304 was defined to collect the on-source events. The background was estimated using the "Reflected Region" method (Aharonian et al. 2006b). Those observations yield an excess of 8800 events, a signal with a significance of 55.7σ calculated following Li & Ma (1983). Using standard cuts an excess of 3612 events with a significance of 68.7σ is found. An independent analysis and calibration (Benbow 2005) yields similar results.

The data from the Large Area Telescope (LAT; Atwood et al. 2008) have been analyzed by using `ScienceTools` version 9.7, which will be publicly available from the *HEASARC* in the future. Events having the highest probability of being photons (class 3, called "diffuse") and coming from zenith angles $< 105°$ (to avoid Earth's albedo) were selected. The diffuse emission along the plane of the Milky Way, mainly due to cosmic-ray interactions with the Galactic interstellar matter, has been modeled using the `54_59Xvarh7S` model prepared with the *GALPROP* code (Strong et al. 2004a, 2004b) which has been refined with *Fermi*–LAT data taken during the first three months of operation. The extragalactic diffuse emission and the residual instrumental background have been modeled as an isotropic power-law component and included in the fit. Photons were extracted from a region with 10° radius centered on the coordinates of PKS 2155−304 and analyzed with an unbinned maximum likelihood technique (Cash 1979; Mattox et al. 1996) using the `Likelihood` analysis software provided by the LAT team. Because of calibration uncertainties at low energies, data in the 0.2–300 GeV energy band were selected.

A total of 75 ks of exposure was taken with *RXTE*, spread over 10 days coinciding with the HESS observations, and a 6.4 ks exposure with *Swift* was made toward the end of the campaign. The data taken with the Proportional Counter Array (PCA; Jahoda et al. 1996) and the X-ray Telescope (XRT; Burrows et al. 2005) instruments were analyzed using the *HEASOFT 6.5.1* package using the Guest Observer Facility recommended criteria. The XRT data were extracted from a 56″ slice, both for the source and the background. Since the rate was less than 10 Hz, no pile-up is expected in the Windowed Timing (WT) mode.

During the multiwavelength campaign, a total of 106 observations were taken with the 0.8 m ATOM optical telescope (Hauser et al. 2004) located on the HESS site. Integration times between 60 s and 200 s in the Bessel *BVR* filter bands were used. Photometric accuracy is typically between 0.01 and 0.02 mag for *BVR*.

2.1. Spectral Analyses

The HESS time-averaged photon spectrum is derived using a forward-folding maximum likelihood method (Piron et al. 2001). The VHE data are well described by a power law of the form $dN/dE = I_0(E/E_0)^{-\Gamma}$, with a differential flux at $E_0 = 350$ GeV (the fit decorrelation energy) of $I_0 = 10.4 \pm 0.24_{\rm stat} \pm 2.08_{\rm sys} \times 10^{-11}$ cm^{-2} s^{-1} TeV^{-1} and a spectral index $\Gamma = 3.34 \pm 0.05_{\rm stat} \pm 0.1_{\rm sys}$. As before, during nonflaring states of PKS 2155−304, the spectrum, measured with limited event statistics, shows no indication of curvature. The spectral index is similar to that previously measured by HESS when the source was at a comparable flux level, in 2003 (Aharonian et al. 2005a, 2005b) and between 2003 and 2005 (F. Aharonian et al. 2009, in preparation). The VHE spectrum is affected by interactions with the extragalactic background light (EBL) which modifies the intrinsic shape and intensity. Using

[75] Supported by CAPES Foundation, Ministry of Education of Brazil.
[76] Authors to whom any correspondence should be addressed.
[77] European Associated Laboratory for Gamma-Ray Astronomy, jointly supported by CNRS, and MPG.
[78] National Research Council Research Associate.
[79] See, e.g., the online TeVCat catalog http://tevcat.uchicago.edu, which has 22 sources at the time of the writing of this Letter.

the $P0.45$ model (Aharonian et al. 2006a), the intrinsic spectral index is derived to be $\Gamma_{\rm int} \approx 2.5$.

The average *Fermi* spectra over the duration of the campaign are fitted by a simple power law for which $I_0 = (2.42 \pm 0.33_{\rm stat} \pm 0.16_{\rm sys}) \times 10^{-11}$ cm^{-2} s^{-1} MeV^{-1}, $\Gamma = 1.81 \pm 0.11_{\rm stat} \pm 0.09_{\rm sys}$, and $E_0 = 943$ MeV is the energy at which the correlation between the fitted values of Γ and I_0 is minimized. The total exposure is 7.7×10^8 cm^2 s. There is no statistical preference for a broken power law in this data set. The light curve derived for *Fermi* data between MJD 54682−54743 shows a similar state on average as during this campaign, so in order to increase the photon statistics for the spectral fits, those data were included, resulting in an increase of the exposure by a factor of 3.6. The longer data set is then fit by a broken power-law spectrum, which is preferred over the single power law with a significance of 97% using the likelihood ratio test. We obtain a low-energy photon index of $\Gamma_L = 1.61 \pm 0.16_{\rm stat} \pm 0.17_{\rm sys}$, a break energy of $E_{\rm br} = 1.0 \pm 0.3$ GeV, a high-energy index of $\Gamma_H = 1.96 \pm 0.08_{\rm stat} \pm 0.08_{\rm sys}$, and a 0.2–300 GeV flux of $(1.13 \pm 0.05_{\rm stat} \pm 0.11_{\rm sys}) \times 10^{-7}$ cm^{-2} s^{-1}. The *Fermi* spectrum is consistent with the hard photon index of 1.71 ± 0.24 during a flaring episode detected by EGRET (Vestrand et al. 1995), but it differs from the Third EGRET Catalog spectrum (Hartman et al. 1999) where the index is 2.35 ± 0.26.

The 4–10 keV PCA and 0.5–9 keV XRT data were analyzed simultaneously with XSPEC version 12.4.0 (Arnaud 1996), using a broken power-law model and taking into account the uncertainty in the cross-calibrations, as well as the variability across the nonsimultaneous observations, by using a multiplicative factor for each instrument (fixed to 1 for the PCA data) as in Falanga et al. (2006). Using a fixed Galactic hydrogen column of $N_{\rm H} = 1.48 \times 10^{-20}$ cm^{-2}, we obtain a low-energy photon index of $\Gamma_1 = 2.36 \pm 0.01$, a break energy of $E_{\rm br} = 4.44 \pm 0.48$ keV, and a high-energy index of $\Gamma_2 = 2.67 \pm 0.01$, for an unabsorbed 2–10 keV flux of 4.99×10^{-11} erg cm^{-2} s^{-1}, which is approximately two times higher than during the 2003 campaign (Aharonian et al. 2006a). This is similar to the VHE flux increase reported above, while still being well below the high state fluxes reported by Vestrand et al. (1995).

2.2. Light Curves

The light curves from HESS, *Fermi*, *RXTE*, and ATOM are shown in Figure 1, where the HESS runs (∼28 minutes) were combined to derive nightly flux values. The average integrated flux above 200 GeV $(5.56 \pm 0.13_{\rm stat} \pm 1.11_{\rm sys}) \times 10^{-11}$ ph cm^{-2} s^{-1}, corresponds to ∼20% $F_{\rm Crab>200\,GeV}$, or ∼50% higher than the quiescent state of 2003 (Aharonian et al. 2006a) and 70 times lower than its peak flaring flux (Aharonian et al. 2007). The positive excess variance $\sigma^2_{\rm XS}$, indicating variability, allows a fractional rms of $F_{\rm var,VHE} = 23\% \pm 3\%$ (see Vaughan et al. 2003 for definitions of $\sigma^2_{\rm XS}$ and $F_{\rm var}$) to be derived, which is three times less than the high state flaring variability reported by Aharonian et al. (2007). A spectrum was obtained for each night when possible, otherwise two or three nights were combined. No indication of spectral variability was found during those observations, with a limit on the nightly index variations of $\Delta\Gamma < 0.2$.

The *Fermi* light curve shows the photon fluxes for the high energy (HE) range, 0.2–300 GeV, and the photon spectral indices for each interval. Each bin is the result of a power-law fit, using the background values found on the overall time-averaged fit, and centered on the HESS observations. The light curve fit to a constant has a χ^2 probability of $p(\chi^2) = 0.95$, clearly consistent with a constant flux. The normalized excess variance of -0.16 ± 0.09 sets a 90% confidence level limit of $F_{\rm var,HE} \leqslant 20\%$ on the fractional variance (Feldman & Cousins 1998).

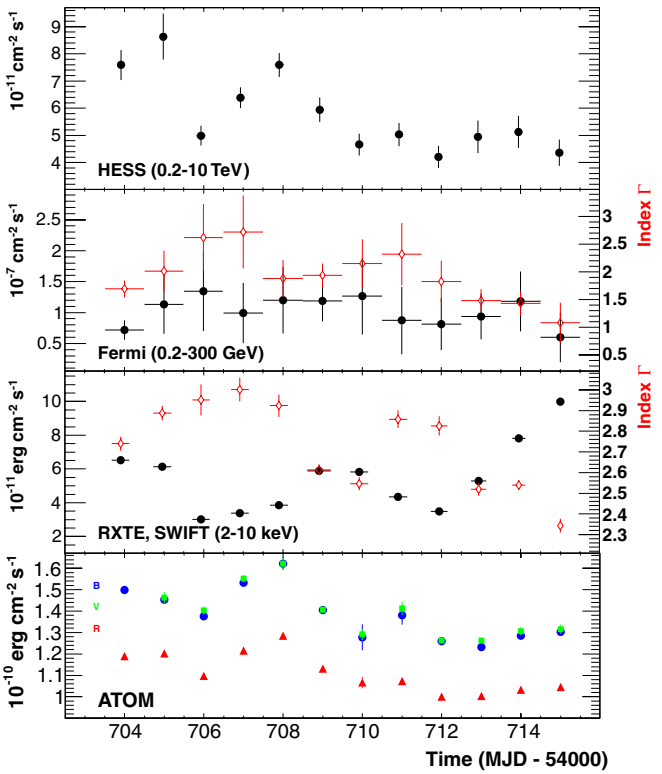

Figure 1. Light curves from (top to bottom): HESS, *Fermi*, *RXTE/Swift*, and ATOM. The *Fermi* and *RXTE/Swift* panels also show the spectral index measurements (red) for each night. Vertical bars show statistical errors only. Horizontal bars represent the integration time and are apparent only for the *RXTE* and *Fermi* data. The ATOM bands are *B* (blue circles), *V* (green squares), and *R* (red squares).

The X-ray light curve, derived from spectral fits of the nightly *RXTE* (and *Swift*) data sets, shows flux doubling episodes on timescales of days, similar to the optical and VHE measurements. The lowest fluxes of ∼3–6 × 10^{-11} erg cm^{-2} s^{-1} are at the same level as those seen in the low state (Aharonian et al. 2005b) but with larger fluctuations, $F_{\rm var,X} = 35\% \pm 0.05\%$. The time history of the fitted spectral indices in Figure 1 show clearly that the X-ray spectrum hardens significantly, $\Delta\Gamma_x \approx 0.5$, as the 2–10 keV flux increases.

The ATOM fluxes are ∼5 times higher than the low state found in Aharonian et al. (2005b), but the *V*-band magnitudes reported here are in the range 12.7–13 which is well on the lower side of the measurements of PKS 2155−304 reported by Foschini et al. (2008) when the source was quoted to be in a low state with *V*-band magnitudes in the range 12–12.7. The host galaxy flux is estimated to be $\approx 10^{-11}$ erg cm^{-2} s^{-1} (Kotilainen et al. 1998), hence most of the optical flux can be attributed to the central AGN. The average fractional rms over all bands is $F_{\rm var,opt} \sim 8\% \pm 0.5\%$. The $B - R$ light curve is compatible with a constant, $p(\chi^2) = 0.66$, indicating little or no optical spectral variability.

3. DISCUSSION

The two-component broadband spectra of high energy-peaked BL Lac objects (HBLs) are typically modeled with syn-

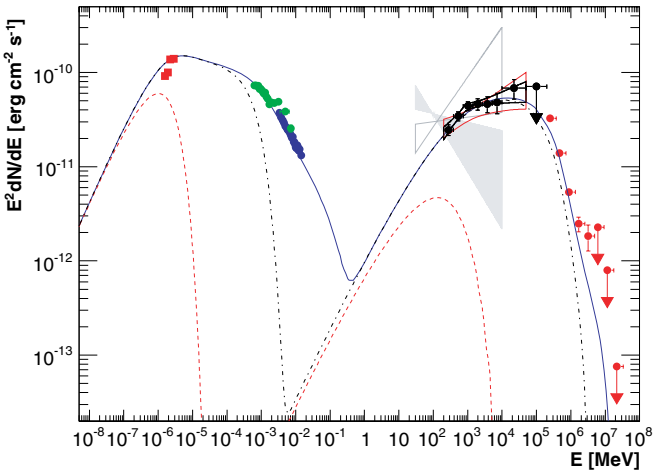

Figure 2. SED of PKS 2155−304. The red butterfly is the *Fermi* spectrum restricted to the MJD 54704−54715 period, while the black butterfly covers MJD 54682−54743. As a cross check of the fit robustness, the differential flux was estimated in eight limited energy bins by a power-law fit (black circles) and are found to be consistent within 1σ of the global fit, including a clear spectral break at ∼1 GeV. The gray points are archival NED data, and the two gray butterflies are EGRET measurements. The solid line is a one-zone SSC model. The dashed and the dot-dashed lines are the same model without electrons above γ_1 and γ_2, respectively. The VHE part is absorbed with the *P*0.45 extragalactic background model described in Aharonian et al. (2006a).

chrotron self-Compton (SSC) scenarios (e.g., Band & Grindlay 1985). Despite the simplicity of these models, they have been successful in reproducing many blazar spectral energy distributions (SEDs) and make definite predictions for the flux and spectral variability that should be seen in the two components. In particular, for typical parameters, the electrons responsible for the X-ray emission also produce the VHE emission; and if the underlying particle distributions were to vary, the resulting flux and spectral changes in the VHE band should be related to variations in the X-rays. In fact, for the 2006 July flare, a nonlinear relationship was seen between the X-ray and VHE bands, though the observed variability patterns do not quite fit the simple SSC model in detail (Costamante 2008).

In Figure 2, we overlay a model SSC calculation that roughly fits the time-averaged SED. The electron distribution model parameters, a three-component power law with indices $p_0 = 1.3$, $p_1 = 3.2$, $p_2 = 4.3$ ($dn/d\gamma \propto \gamma^{-p_i}$), minimal and maximal Lorentz factors $\gamma_{\rm min} = 1$ and $\gamma_{\rm max} = 10^{6.5}$, break electron Lorentz factors $\gamma_1 = 1.4\times10^4$, $\gamma_2 = 2.3\times10^5$, and total electron number $N_{\rm tot} = 6.8 \times 10^{51}$, have been set to reproduce the shape of the lower energy component of the SED. The overall SED is then adjusted with the remaining parameters: radius of the emitting region in the comoving frame, $R = 1.5 \times 10^{17}$ cm; bulk Doppler factor, $\delta = 32$; magnetic field, $B = 0.018$ G. Even though we regard this fit as a "straw-man" model, it is perhaps reassuring that the joint *Fermi*–HESS time-averaged spectra can be reasonably well described as SSC emission. Katarzyński et al. (2008) found similar values for R, B, and δ in their SSC description of a steady large jet component in the SED of PKS 2155−304.

Some features of this model calculation are particularly noteworthy. The electrons that produce the synchrotron X-ray emission have Lorentz factors $> \gamma_2$. When the power-law component for those electrons is omitted from the calculation, the dot-dashed curve in Figure 2 results. For this particular set of parameters, the electrons that produce the X-rays have higher energies than the electrons that produce the VHE emission. Furthermore, the lack of a significant impact on the shape of the SSC component when those electrons are removed indicates that Klein–Nishina effects suppress any significant contribution by those electrons to the emission at ∼TeV energies.

These features of this calculation allow that there need not be a correlation between the X-ray and VHE fluxes; and in fact, this is what is observed. In contrast with the 2006 July flare, we do not find any evidence of flux correlation between the X-ray and HESS bands with a Pearson's r of 0.12 ± 0.1 between these bands. Furthermore, the 2–10 keV X-ray spectra show spectral variability consistent with an underlying electron distribution for which the cooling timescales are of order the flux variability timescales, i.e., the spectra are softer when the flux is lower, with changes in photon index of $\Delta\Gamma_x \approx 0.5$ (Figure 1); whereas, the VHE emission shows no evidence for significant spectral variability despite flux variations of a factor of 2. Since radiative cooling timescales vary inversely with electron energy, this supports the conclusion that the electrons responsible for the synchrotron emission in the X-ray band have higher energies than the electrons that produce the inverse-Compton emission in the VHE range, assuming they are part of the same overall nonthermal distribution.

Even though this all fits in with our straw-man SED calculation, the variability patterns in the optical, X-ray, HE, and VHE bands suggest a much more complex situation. In the absence of spectral variability, the mechanisms that would produce the observed flux variability in the VHE band are rather constrained. Increases in flux could be driven by injection of particles with a constant spectral shape, and decreases in flux could be caused by particle escape from the emitting region or by expansion (adiabatic) losses, assuming those latter two processes can operate independent of particle energy. However, since the electrons that produce the VHE emission must be in the weak radiative cooling regime, a more natural mechanism for the flux variability would be that changes in the seed photon density are driving the variability. Comparing the daily flux values in the optical and the VHE bands, we find indications of fairly strong correlations that suggest that the optical emission provides the target photons for the IC emission. In the B, V, and R bands, the correlations with the HESS fluxes have Pearson's r values in the range 0.77–0.86 with uncertainties $\leqslant 0.09$. This correlated behavior is readily apparent in the light curves shown in Figure 1, and these results provide the first quantitative evidence of correlated variability between the optical and VHE bands on these timescales for an HBL.[80] Confirmation of this behavior, not only from this source but also from other VHE emitting blazars in a low state, would provide important constraints on emission models for these objects.

In the context of a single-zone SSC model, we would expect that any flux variability in the optical bands should also appear as variability in the *Fermi*–LAT energy range. To illustrate this, we plot, as the dashed curve in Figure 2, the SED that results if we omit contributions from electrons with energies $> \gamma_1$. For the original model parameters, the electrons that produce the optical-soft X-ray emission also produce the bulk of the IC component, including the HE and VHE emission. Since we do not find any indication of a correlation between the optical and HE fluxes, this suggests that the optical emission may arise from a separate population of electrons than those responsible for the

[80] Donnarumma et al. (2008) mention possible correlated variability in the recent 2008 June flare of Mrk 421 in a high state.

HE and VHE emission. If so, then these electrons probably also occupy a distinct physical region with different physical parameters (magnetic field, size scale, bulk Lorentz factor). Multizone SSC models of this kind have already been proposed to account for the "orphan" γ-ray flare in 1ES 1959+650 during 2002 May (Krawczynski et al. 2004).

Although the 0.2–300 GeV photon fluxes measured by *Fermi* are consistent with being constant, we find more significant variations of the photon spectral index in the daily analyses ($p(\chi^2) = 0.19$). The fitted values range from fairly soft, $\Gamma = 2.7 \pm 0.7$, to extremely hard, $\Gamma = 1.1 \pm 0.4$. These values, along with the constant, intrinsic VHE index of $\Gamma_{\rm VHE} \approx 2.5$ derived from the HESS data, imply spectral breaks between the HE and VHE bands of $\Delta\Gamma$ as large as 1.4. Very sharp spectral breaks ($\Delta\Gamma \gtrsim 1$) would require rather narrow electron distributions and would therefore pose difficulties in fitting a broad lower energy component in the context of a single-zone model. Interestingly, we find a significant anticorrelation between the nightly X-ray fluxes and the *Fermi*–LAT spectral indices of $r_{X\Gamma} = -0.80 \pm 0.15$. A fit to a linear model is preferred over a constant at the 2.6σ level, with a slope of -0.14 ± 0.05. If the electrons that produce the X-rays are at higher energies than those that produce the TeV emission, the cause for such a correlation would be difficult to understand. An important caveat in considering these results is that the *Fermi* coverage for PKS 2155−304 was relatively uniform over each 24 hr period, whereas the optical, X-ray, and VHE observations were restricted to 4–6 hr intervals each night. Hence, the *Fermi* observations are not strictly simultaneous with the other measurements, so it is possible that some of the observed HE spectral variability occurred outside of the nightly observing windows.

As the first multiwavelength campaign of an HBL that includes *Fermi* and an ACT instrument, these observations have yielded results that strongly challenge the standard models for these sources. Having caught PKS 2155−304 in a low state, we see that its spectral and variability properties are significantly different than its flaring, high state behavior. The variability patterns, in particular, defy easy explanation by the usual SSC models and should provide valuable constraints for models that attempt to describe the emission mechanisms in blazar jets.

The full HESS and *Fermi*–LAT acknowledgements can be found on Web sites http://www.mpi-hd.mpg.de/hfm/HESS/acknowledgements and http://www-glast.stanford.edu/acknowledgements.

REFERENCES

Aharonian, F., et al. (HESS Collaboration) 2004, Astropart. Phys., 22, 109
Aharonian, F., et al. (HESS Collaboration) 2005a, A&A, 430, 865
Aharonian, F., et al. (HESS Collaboration) 2005b, A&A, 442, 895
Aharonian, F., et al. (HESS Collaboration) 2006a, Nature, 440, 20
Aharonian, F., et al. (HESS Collaboration) 2006b, A&A, 457, 899
Aharonian, F., et al. (HESS Collaboration) 2007, ApJ, 664, L71
Arnaud, K. A. 1996, in ASP Conf. Ser. 101, Astronomical Data Analysis Software and Systems V, ed. G. H. Jacoby & J. Barnes (San Francisco, CA: ASP), 17
Atwood, W. B., et al. 2008, ApJ, submitted (arXiv:0902.1089)
Band, D. L., & Grindlay, J. E. 1985, ApJ, 298, 128
Benbow, W. 2005, Proc. Towards a Network of Atmospheric Cherenkov Detectors VII (Palaiseau), 163
Burrows, D. N., et al. 2005, Space Sci. Rev., 120, 165
Cash, W. 1979, ApJ, 228, 939
Costamante, L. (HESS Collaboration) 2008, Int. J. Mod. Phys. D, 17, 1449
Donnarumma, I., et al. 2008, ApJ, 691, 13
Falanga, M., Belloni, T., & Campana, S. 2006, A&A, L5, 456
Feldman, G. J., & Cousins, R. D. 1998, Phys. Rev. D, 57, 3873
Foschini, L., et al. 2008, A&A, 484, 35
Hartman, R. C., et al. 1999, ApJS, 123, 79
Hauser, M., et al. 2004, Astron. Nachr., 325, 659
Jahoda, K., et al. 1996, Proc. SPIE, 2808, 59
Katarzyński, K., Lenain, J.-P., Zech, A., Boisson, C., & Sol, H. 2008, MNRAS, 390, 371
Kotilainen, J. K., Falomo, R., & Scarpa, R. 1998, A&A, 336, 479
Krawczynski, H., et al. 2004, ApJ, 601, 151
Li, T.-P., & Ma, Y.-Q. 1983, ApJ, 272, 317L
Mattox, J. R., et al. 1996, ApJ, 461, 396
Piron, F., et al. 2001, A&A, 374, 895
Strong, A. W., Moskalenko, I. V., & Reimer, O. 2004a, ApJ, 613, 962
Strong, A. W., Moskalenko, I. V., Reimer, O., Digel, S., & Diehl, R. 2004b, A&A, 422, L47
Vaughan, S., Edelson, R., Warwick, R. S., & Uttley, P. 2003, MNRAS, 345, 1271
Vestrand, W. T., Stacy, J. G., & Sreekumar, P. 1995, ApJ, 454, 93